Biology Direct

RESEARCH

Open Access

# Sorafenib-induced macrophage extracellular traps via ARHGDIG/IL4/PADI4 axis confer drug resistance through inhibiting ferroptosis in hepatocellular carcinoma

Xiangbo Huang[1,2], Nan Yi[1,2], Pengfei Zhu[1,2], Jian Gao[3*] and Jun Lv[4*]

## Abstract

**Background** Hepatocellular carcinoma (HCC) is one of the most common as well as leading causes of mortality worldwide, and sorafenib is the first-line treatment in HCC patients. Unfortunately, drug resistance to sorafenib often develops. However, the underlying mechanism remains unclear. Here, we reveal the important role of macrophage extracellular traps (METs)-mediated crosstalk between macrophages and tumor cells in sorafenib resistance.

**Methods** METs in HCC tumor tissues were detected using immunofluorescence. The concentrations of MPO-DNA, elastase and cytokines were measured using ELISA. The mRNA expression levels of genes were confirmed by qRT-PCR. The siRNAs were conducted to knock ARHGDIG in Hepa1-6 and Hep3B cells. Western Blot assay was performed to determine protein expression of Rho GDP dissociation inhibitor gamma (ARHGDIG, or RHOGDI-3), PADI2, and PADI4. Cell viability and migration were evaluated by CCK-8 assay and transwell assay, respectively. Cell ferroptosis was assessed by measurement of $Fe^{2+}$ concentration, flow cytometry assay of lipid ROS, and western blot assay of GPX4. The functions of sorafenib, DNase I, IL4 neutralization antibody and GPX4 in tumor growth were explored through in vivo experiments.

**Results** Sorafenib induced MET formation in M2 macrophages rather than M1 macrophages derived from both human and mice. In Hepa1-6 HCC mice, METs clearance by DNase I improved response to sorafenib therapy, detected by tumor weight, tumor growth curve, tumor volume, and survival. By screening candidate cytokines that affect macrophage function, we found that sorafenib-promoting IL4 secretion by HCC cells plays a crucial role in sorafenib-induced MET formation. Understanding the critical role of IL4 in sorafenib-induced MET formation led us to find that IL4 neutralization significantly improved the efficiency of sorafenib in HCC models. Mechanistically, we discovered that sorafenib increased the expression of ARHGDIG in HCC cells, which led to the release of IL4. In M2 macrophages, IL4 triggered MET formation by elevating the mRNA and protein expression of peptidyl arginine deiminase 4 (PADI4) rather than PADI2. In HCC models, GSK484 inhibition of PADI4 could consistently weaken sorafenib resistance and improve sorafenib efficiency. Importantly, we discovered that METs contribute to sorafenib resistance by inhibiting the ferroptosis of HCC cells. Meanwhile, PADI4 inhibition or DNase I could reverse the sorafenib resistance caused by METs-inhibiting ferroptosis of HCC cells.

*Correspondence:
Jian Gao
gaojian@renji.com
Jun Lv
fcclvj@zzu.edu.cn
Full list of author information is available at the end of the article

**Conclusion** Our study concludes that sorafenib-induced METs inhibit the ferroptosis of tumor cells, suggesting that targeting the IL4/PADI4/METs axis in HCC could reduce or prevent sorafenib resistance.

**Keywords** Hepatocellular carcinoma, Sorafenib, Macrophage extracellular traps, ARHGDIG, IL4, PADI4, Ferroptosis

## Introduction

Liver cancer is ranked third in terms of mortality and seventh in terms of morbidity among different malignancies, according to global cancer data for 2020 [1]. Hepatocellular carcinoma (HCC) accounts for 75–85% of primary liver cancers and remains the leading cause of cancer-related death [1, 2]. Sorafenib is currently the first-line therapy in HCC, but the development of sorafenib resistance is becoming increasingly common [3]. Sorafenib is a multikinase inhibitor capable of inducing ferroptosis [4] and it can exert therapeutic effects by modulating ferroptosis. Ferroptosis is a form of cell death characterized by iron dependence and lipid peroxidation. Furthermore, ferroptosis unleashes new possibilities for cancer therapy, especially HCC [5], but the resistance to sorafenib-induced ferroptosis remains a major challenge. Therefore, discovering the mechanism underlying resistance to ferroptosis is necessary to improve the prognosis after sorafenib treatment [6, 7].

Tumor-associated macrophages (TAMs) are essential in sorafenib therapy and resistance. TAMs are abundant in the tumor microenvironment of HCC [8, 9], and the expression profile and mediator secretion of TAMs are highly immunosuppressive and contribute to the therapy resistance of HCC [10, 11]. In liver cancer, M2 TAMs contribute to cancer cell stemness, facilitate cancer cell proliferation, aggressiveness, and metastasis, and stimulate angiogenesis [8, 12]. Sorafenib treatment increased the number of M2-like TAMs in the tumor microenvironment of HCC [13]. Depleting TAM or repolarizing M2 to M1 macrophages could improve sorafenib sensitivity and efficacy in HCC [14], indicating that TAM, predominantly M2 macrophages, plays a role in sorafenib resistance. Macrophage-derived secretary molecules, including hepatocyte growth factor (HGF) [12], insulin-like growth factor (IGF) [15], and CXCL1/2 [16], are involved in the resistance against sorafenib. Nevertheless, the mechanisms underlying TAM-related sorafenib resistance remain far from clear [17].

Macrophage extracellular traps (METs) are a network structure formed by depolymerized chromatin released by activated macrophages [18–21]. Its skeleton comprises double-stranded DNA, which combines histones, myeloperoxidase (MPO), and elastase. The latest research has found that MET formation is critical for promoting tumor progression. The prognosis is poor for elevated MPO-DNA in tumor tissues and serum, such as in patients with colorectal cancer with liver metastases [22], advanced gastric cancer (GC) [23], and diffuse large B-cell lymphoma [24]. Clinical studies have found that low levels of METs in tumor tissues of patients with pancreatic neuroendocrine cancer are an independent prognostic factor for 3-year recurrence-free survival [18]. In colon cancer, patients with high levels of METs in tumor tissue are more likely to develop distant metastasis, and high levels of METs in tumor tissues have a lower 5-year survival rate [19]. However, the role of METs in HCC still needs to be discovered.

In this study, we found the induction of MET formation in HCC during sorafenib treatment and, more importantly, MET reduced therapeutic response against sorafenib. We further discovered that sorafenib administration increased Rho GDP dissociation inhibitor gamma (ARHGDIG, or RHOGDI-3) expression, which promoted interleukin 4 (IL4) secretion from HCC cells. Consequently, IL4 increased peptidyl arginine deiminase 4 (PADI4) expression, which in turn caused MET formation. METs inhibited sorafenib-induced ferroptosis of HCC cells to impart sorafenib resistance. Additionally, we found that sorafenib combined with MET inhibition therapy provides a much more potent therapeutic effect than either treatment alone. We have thus discovered an IL4-PADI4-METs axis that contributes to sorafenib resistance by inhibiting the sorafenib-induced ferroptosis of HCC cells, opening new avenues for further research and potential therapeutic strategies.

## Materials and methods

### Cell culture

Human HCC cell line Hep3B and mouse HCC cell line Hepa1-6 were cultured in DMEM supplemented with 10% fetal bovine serum (FBS), 100 U/ml penicillin, and 100 mg/ml streptomycin. The cells were passaged every 2–3 days when they achieved around 80% confluency. Human monocyte cells THP-1 were cultured in RPMI-1640 medium supplemented with 10% (v/v) FBS, 0.05 mM of 2-mercaptoethanol,100 U/ml penicillin, and 100 mg/ml streptomycin. THP-1 monocytes were differentiated as previous report [25]. THP-1 monocytes were polarized to M0 macrophage by 24 h incubation with 5 ng/mL phorbol 12-myristate 13-acetate (PMA; Sigma-Aldrich, #P8139). Mo macrophages were polarized in M1 macrophages by incubation with 20 ng/ml of IFN-γ (R&D system, #285-IF) and 100 ng/ml of LPS (Sigma-Aldrich,

L2880). Based on M0 macrophage, 20 ng/ml of IL4 (R&D Systems, #204-IL-010) and 20 ng/ml of interleukin 13 (R&D Systems, 213-ILB-025) were used to induce them to polarize into M2 macrophage. All cells were maintained in an incubator at 37 °C and 5% CO2.

#### Detection of METs in tumor-infiltrating macrophages

The single-cell suspensions were prepared from the tumor tissues of Hepa1-6-bearing HCC mice. Macrophages were then isolated using the Anti-F4/80 MicroBeads UltraPure (Miltenyi Biotec, #130-110-443) according to the manufacturer's introductions. The collected cells were fixed with 4% paraformaldehyde and stained with anti-Cit-H3 (Abcam, #ab281584) and anti-F4/80 (Abcam, #ab6640) antibodies followed by fluorescence-labeled second antibodies and counterstained with DAPI (AbMole, #M5106). The samples were observed under a Leica TCS SP8 confocal microscope (Leica).

#### *In vitro treatment*

Hepa1-6 cells were treated with sorafenib (MedChemExpress, #HY-10201) at 5 μM for 12 h, and Hep3B cells were treated with sorafenib at 2.5 μM for 12 h. M2-mBMDM and M2-THP-1 were treated with recombinant murine (PeproTech, #214-14) IL-4 or human IL-4 (PeproTech, #200–04) respectively. In the in vitro inhibition, the information of IL4 inhibitors are as follows: Anti-murine IL-4 neutralizing antibody (10 μg $ml^{-1}$; BioXCell, clone: 11B11, #BE0045) [26], Anti-human IL-4 neutralizing antibody (10 μg $ml^{-1}$; BioXCell, clone: MP4-25D2, # BE0240) [27]. The PADI4 inhibitor is GSK484 (10 μM; Cayman Chemicals, #1,652,591-81-5) [28]. The ferroptosis inhibitor is deferoxamine (DFO) (100 μM, 24 h; MedChemExpress, #HY-B1625), a selective iron chelator.

#### Mouse bone marrow-derived macrophages (mBMDMs) culture and polarization

mBMDMs were isolated from euthanized mice of 8-week-old, according to previous report [29]. Briefly, femurs from mice were cut in a sterile glass and the bone marrow cavity was flushed out with chilled PBS, followed by red cell lysis. Once isolated, the mBMDMs were cultured in DMEM containing 10% FBS, and 1% penicillin/streptomycin. To initiate macrophage differentiation, the medium was supplemented with 100 ng/ml of recombinant murine M-CSF (PeproTech, #315–02) for 7 days. To induce M1-like polarization, mBMDMs were stimulated with recombinant murine GM-CSF (10 ng/ml; PeproTech, # 315–03) for 6 days followed by IFN-γ (20 ng/ml; Sigma-Aldrich, #I4777) and LPS (100 ng/ml) for 24 h. To induce M2-like polarization, mBMDMs were stimulated with M-CSF (10 ng/ml) for 6 days followed by M-CSF (10 ng/ml) and IL4 (20 ng/ml; PeproTech, #214–14) for 24 h.

#### Coculture experiments

The co-culture experiments were conducted using the UniWells™ Horizontal Co-Culture Plate (Wako, #384-14,421) as previous description [30]. Hep1-6 or Hep3B cells ($6\times10^3$/well) were plated in one chamber in 6-well plates, and THP-1 or M2-mBMDM cells ($1\times10^5$) were seeded in another chamber of the co-culture plate. The cells were cocultured in 0.5% (v/v) FBS medium at 37 °C and 5% $CO_2$ for 24 h.

#### MPO-DNA complex assay

MPO-DNA complexes in mouse plasma and cell culture supernatants were detected using a capture ELISA as previous reports [31–34]. Briefly, as the capturing antibody, we used an anti-MPO antibody (R&D, #AF3667). The plasma or supernatants was added in combination with the peroxidase-labeled anti-DNA monoclonal antibody (component No.2 of the commercial cell death detection ELISA kit; Roche, #11-774-425-002). The reaction was stopped with 1 N hydrochloric acid and the plate read at 405 nm with 490 nm background subtraction using the Synergy 2 microplate reader (BioTek, Winooski, VT, USA).

#### Cytokine measurements by ELISA

The enzyme-linked immunosorbent assay (ELISA) was used to measure mouse elastase (Mouse Neutrophil Elastase/ELA2 ELISA Kit, RayBiotech, #ELM-ELA2), human elastase (Human Neutrophil Elastase ELISA Kit, RayBiotech, #ELH-NEUTRO), mouse IL4 (Mouse IL-4 ELISA Kit, Abcam, #ab100710), and human IL4 (Human IL-4 ELISA Kit, RayBiotech, #ELH-IL4) in supernatant collected from cell culture dishes or flasks, according to the manufacturer's instructions.

#### siRNA transfection

The small interfering RNA (siRNA) knocking ARHGDIG was designed using BLOCK-iT™ RNAi Designer (https://rnaidesigner.thermofisher.com/rnaiexpress/setOption.do?designO). The targeting sequences of siRNA were as follows: homo ARHGDIG, 5'- AGATTGTCAGCGGCC TCAAGTGTCT-3'; mus ARHGDIG, 5'- CCAGGGCCT ATCATCATGGACCTTA-3'. According to the manufacture' guidelines, we used Lipofectamine RNAiMAX (Invitrogen, #13,778,030) and Opti-MEM (Gibco, #31,985,070) to transiently transfect Hep3B and Hepa1-6 cells with respective siRNA. After 72 h, the cells were used for subsequent experiments.

### Cell counting kit-8 (CCK-8) assay

The cells were seeded in a 96-well plate (100 μL/well). After treatment for 24, 48, and 72 h, 10 μL of the Cell Counting Kit-8 (CCK-8, Sigma-Aldrich, #96,992) solution was added to each well, and the 96-well plate was subsequently incubated at 37 °C for 2 h in the incubator. The optical density (OD) was measured at 450 nm to determine the cell viability on a using the Synergy 2 microplate reader (BioTek). The assay was performed at least in triplicate.

### HCC cell migration assays

This assay was performed using Corning incorporated costar transwell plates that contained polycarbonate filters with 8-μm pores (Corning, #3422) according to the manufacturer's instructions. Briefly, $10^5$ Hepa1-6 or Hep3B cells in 200 μL of serum-free media were seeded into the upper cell culture inserts, which were placed in the 24-well plates containing 600 μL of complete media supplemented with 10% FBS and incubated at 37 °C, 5% CO2. 24 h later the migrated cells in the bottom of the inserts were then fixed in 4% paraformaldehyd for 30 min and stained with 1% crystal violet (Sigma-Aldrich, #548-62-9), and nonmigrated cells were removed from the inserts using cotton-tipped swabs. Finally, the membranes were visualized using an OLYMPUS microscope system (Tokyo, Japan). The number of migrated cells in each field was quantified by counting 3 wells/group.

### Western blot assay

Protein samples were separated using SDS-PAGE and transferred onto polyvinylidene difluoride (PVDF) membranes. The membranes were blocked with 5% nonfat milk for 2 h at room temperature, followed by incubation with primary antibodies. Primary antibodies specific to rabbit anti-ARHGDIG (Invitrogen, # PA5-75,561), anti-IL4 (Invitrogen, #PA5-25,165), anti-PADI2 (Invitrogen, #PA5-106,273), anti-PADI4 (Invitrogen, #PA5-22,317), anti-GPX4 (Invitrogen, #PA5-120,674), and anti-β-actin (1:2,000; Invitrogen, #PA1-183) from Thermofisher Scientific were used. The samples were then incubated with horseradish peroxidase-conjugated goat anti-rabbit IgG secondary antibody (Invitrogen, #31,460) for 1 h at room temperature. After washing the membrane, the protein band was detected using the ChemiDoc™ XRS + system (Bio-Rad, Hercules, CA, USA).

### Xenografts and tumorigenesis assays

To construct a subcutaneous HCC model, Hep1-6 cells ($5 \times 10^6$ cells/mouse) were resuspended in serum-free media and were subcutaneously inoculated into the right flanks of 5-week-old male C57BL/6 mice. For sorafenib treatment, Hepa1-6 tumor-bearing mice were administrated with sorafenib (30 mg/kg/day, oral gavage) [35, 36]. To digest METs DNA, tumor-bearing mice were intravenously injected with DNase I (50 μg/mouse, twice/week; Roche, #11,284,932,001), and the negative controls were administered the same volume of saline. For IL4 inhibition mice were intraperitoneally injected with InVivoMAb anti-mouse IL-4 (25 μg/mice/two days; BioXCell, clone: 11B11, #BE0045) to neutralize the biological activity of IL4 [37, 38], and the negative controls received an equal amount of InVivoMAb rat IgG1 isotype control (BioXCell, clone: HRPN, #BE0088). For PADI4 inhibition mice were treated daily by intraperitoneal injections of GSK484 (4 mg/kg; Cayman Chemicals, # 1,652,591–81-5), and the negative controls were administered the same volume of saline [39]. All treatments start at 1 week after tumor implantation and take 3 weeks.

Body weight and tumor growth were monitored twice every week. The tumor volumes were measured using a caliper and calculated using the following formula: tumor volume $(mm^3) = (\text{length [mm]}) \times (\text{width [mm]})^2 \times 0.5$. The endpoint is reaching one of the following criteria: (i) body weight loss of > 15%, (ii) tumor volume exceeded 800 $mm^3$, (iii) a combination of body weight loss of > 10% and tumor volume exceeded 700 $mm^3$, (iv) signs of unease and pain [40].

All procedures involving animals were approved by the Animal Care and Use Committee of the First Affiliated Hospital of Zhengzhou University.

### RNA isolation and quantitative reverse transcription polymerase chain reaction (qRT-PCR)

Total RNA of the cultured cells was isolated with TRIzol reagent (Invitrogen). The cDNA was obtained via the PrimeScript™ RT Master Mix (Perfect Real Time) kit (TaKaRa, # RR036A), which was conducted as follows: 37 °C for 15 min, 85 °C for 5 s, and 4 °C hold. The primers of human target genes for qRT-PCR were provided in Table S2. The primers of mouse IL4: Forward, 5'-GGT CTCAACCCCCAGCTAGT-3'; Reverse, 5'-GCCGAT GATCTCTCTCAAGTGAT-3'. Subsequently, qRT-PCR were detected by LightCycler® RNA Amplification Kit SYBR Green I (Roche, # 12,015,137,001) in the QuantStudio™ 7 Flex (AppliedBiosystems, Thermofisher scientific). qRT-PCR was initiated by a hold stage of 50 °C for 2 min and 95 °C for 10 min; for the PCR stage, the denaturation was at 95 °C for 15 s followed by annealing/extension at 60 °C for 1 min, the number of cycles was 40. The relative levels of genes were calculated and normalized to the internal control β-actin with the Eq. $2^{-\Delta Ct}$, in which ΔCt (cycle threshold) = Ct gene − Ct control. All genes were assayed at least in triplicate.

#### $Fe^{2+}$ concentration measurement

Hepa1-6 and Hep3B cells were seeded on 6-well plates and cocultured with conditioned medium-treated M2-mBMDM or M2-THP-1 respectively. The levels of intracellular $Fe^{2+}$ were detected using the Iron Assay kit (Colorimetric) (Abcam, #ab83366) according to the protocol. The absorbance was measured at 593 nm using the Synergy 2 microplate reader (BioTek, Winooski, VT, USA).

#### Lipid peroxidation measurement

After incubation with the media of conditioned medium-treated M2-mBMDM or M2-THP-1 respectively, Hepa1-6 and Hep3B cells were harvested and resuspended in PBS containing BODIPY™ 581/591 C11 (Lipid Peroxidation Sensor) (Invitrogen, #D3861). Cells were incubated for 1 h min at 4 °C avoid light. Lipid peroxidation (Lipid ROS) was measured by the flow cytometer FACS Celesta (BD, Franklin Lakes, New Jersey, U.S.). 10,000 single cells per tube were analyzed. As previous description [41], oxidation of the C11-BODIPY fluorophore shifts the fluorescence emission from red to green, and the change in the ratio of the oxidised and reduced form CH1 (ox)/CH2 (red) was used as an indicator of an increase in lipid peroxidation.

#### Statistical analysis

Data were expressed as the mean ± SD. All statistical analyses in this study were performed using GraphPad Prism (GraphPad, La Jolla, CA, USA). Differences between two groups were analyzed using the unpaired Student's t test (two-tailed tests). Log-rank (Mantel-Cox) test was used for survival analysis. The difference was statistically significant at $P$ value < 0.05. ns, $p \geq 0.05$; *, $p < 0.05$; **, $p < 0.01$; ***, $p < 0.001$.

## Results

#### Sorafenib induced M2 macrophage-derived METs in the tumor environment of HCC

To investigate the effects of sorafenib therapy on METs, we analyzed the MET levels in isolated macrophages from the tumor tissues of Hepa1-6-bearing HCC mice by immunofluorescence staining for citrullinated histone H3 (Cit-H3), a specific marker for extracellular traps, on day 25 post-treatment (three days following the previous dose of sorafenib). It was found that sorafenib therapy led to the formation of more METs in tumor tissues (Fig. 1A). Sorafenib-induced formation of extracellular traps was further confirmed by the elevated levels of peripheral MPO-DNA, another marker for extracellular traps [42], in sorafenib-treated Hepa1-6 tumor-bearing mice (Fig. 1B). Neutrophils and macrophages are considered as the main sources of extracellular traps. Sorafenib treatment could still increase the level of peripheral MPO-DNA in neutrophil-depleted mice but failed to elevate its level in macrophage-depleted mice (Fig. 1B), suggesting the critical contribution of macrophages rather than neutrophils in sorafenib-induced extracellular trap formation in HCC-bearing mice. To explore the effect of sorafenib on METs, we performed in vitro MET formation experiments. The treatment of either macrophages (mouse bone marrow-derived macrophage (mBMDM) or human THP-1-derived macrophages) or HCC cells (Hepa1-6 or Hep3B) with sorafenib did not change the MPO-DNA levels in their supernatants (Fig. 1C and S1A-B). Interestingly, there was a significant increase in MPO-DNA level when mBMDM or THP-1-derived macrophages were cultured in the conditioned medium (CM) from sorafenib-treated HCC cells (Fig. 1D). However, the CM from sorafenib-treated HCC cells failed to significantly enhance extracellular DNA trap formation in mouse bone marrow-derived neutrophils (mBMDNs) or human neutrophil-differentiated HL-60 cells (Fig. 1E). These results demonstrated the enhanced MET formation induced by sorafenib in HCC and suggested the involvement of secretory molecular-mediated crosstalk between HCC cells and macrophage in sorafenib-induced MET formation. Additionally, we found that the CM from sorafenib-treated HCC cells was more potent in inducing MET in M2-poralized macrophages rather than M1-poralized macrophages, indicating M2 macrophages as the main source of sorafenib-induced METs (Fig. 1F, G).

#### METs mediated sorafenib resistance in HCC in vivo

DNase I was usually used to degrade extracellular traps [43]. To further explore the impact of METs on sorafenib treatment, the Hepa1-6 tumor-bearing mice were administrated with saline (NC), Sora, DNase I, or Sora + DNase I. The results showed that, at the time of sacrifice, the tumors treated with sorafenib or DNase I alone were significantly smaller than the saline-treated control tumors (Fig. 2A, B). Notably, the combination therapy led to the smallest tumors among these groups (Fig. 2A) and an almost 66% decrease in tumor weight as compared to the sorafenib alone group (Fig. 2B). In an independent replicate experiment, we monitored the tumor volumes of each group after treatment. Although sorafenib or DNase I treatment alone slowed the growth of tumors as compared to control tumors (growth curve), we did not observe tumor regression in individual mice of single treatment groups (Fig. 2C, D). Surprisingly, the combination therapy caused tumor regression in one-third of mice (2/6) (Fig. 2C). On Day 25 after the first injection, the sorafenib exhibited a 47% reduction in the mean tumor volume compared to the NC group, but the

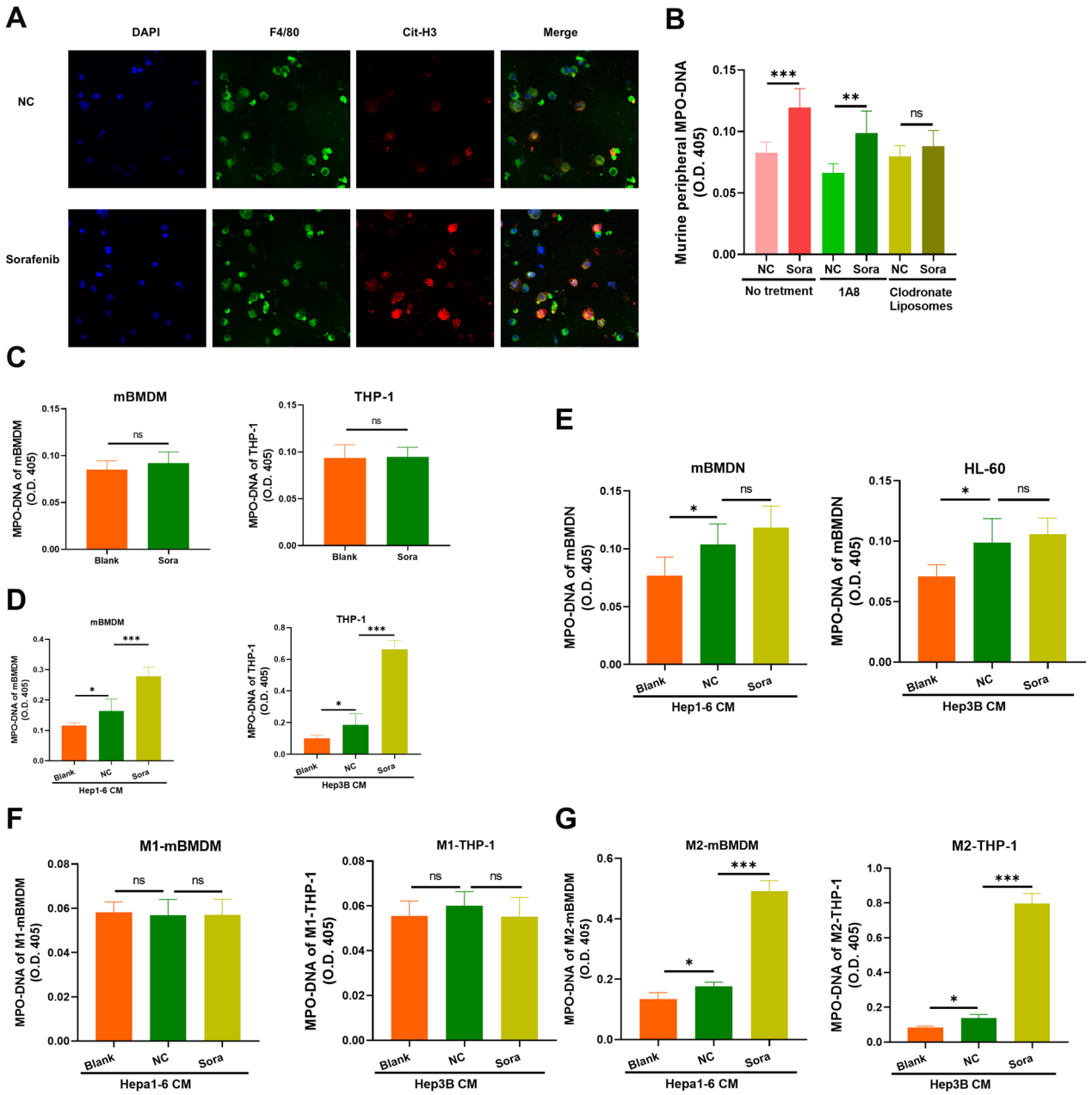


**Fig. 1** The impact of sorafenib on MET formation in the tumor environment of HCC. **A** Representative immunofluorescence images of F4/80$^{+}$CitH3$^{+}$cells in isolated macrophages from tumor tissues (40×). Blue, DAPI; Green, F4/80 positive; Red, Cit-H3 positive. **B** The impact of neutrophils and macrophages on extracellular traps in Hep1-6-bearing HCC C57BL/6 mice. NC: negative control with saline treatment. Sora: treatment with sorafenib. 1A8: anti-Ly6G for depleting murine neutrophils. **C** ELISA detection of the MPO-DNA concentration in the supernatant of mouse bone marrow-derived macrophage (mBMDM) and THP-1 cells that were treated by sorafenib (Sora). Blank: no treatment. ELISA detection of the MPO-DNA concentration in the supernatant of **D** mBMDM and THP-1 cells, and **E** mouse bone marrow-derived neutrophil (mBMDN) and HL-60 cells that were treated with HCC cell media. Blank: no treatment. NC: media of Hepa1-6 or Hep3B. Sora: media of Hepa1-6 or Hep3B treated by sorafenib. Clodronate liposomes were used for depleting murine macrophages. ELISA detection of the MPO-DNA concentration in the supernatant of (**F**) M1-mBMDM and M1-THP-1 cells, and **G** M2-mBMDM and M2-THP-1 cells that were treated with HCC cell media. Blank: no treatment. NC: media of Hepa1-6 or Hep3B. Sora: media of Hepa1-6 or Hep3B treated by sorafenib. n = 6 (**B**–**G**). Data represent the mean ± standard deviation (SD) of ≥ three independent experiments. ns, $p \geq 0.05$; *, $p < 0.05$; **, $p < 0.01$; ***, $p < 0.001$

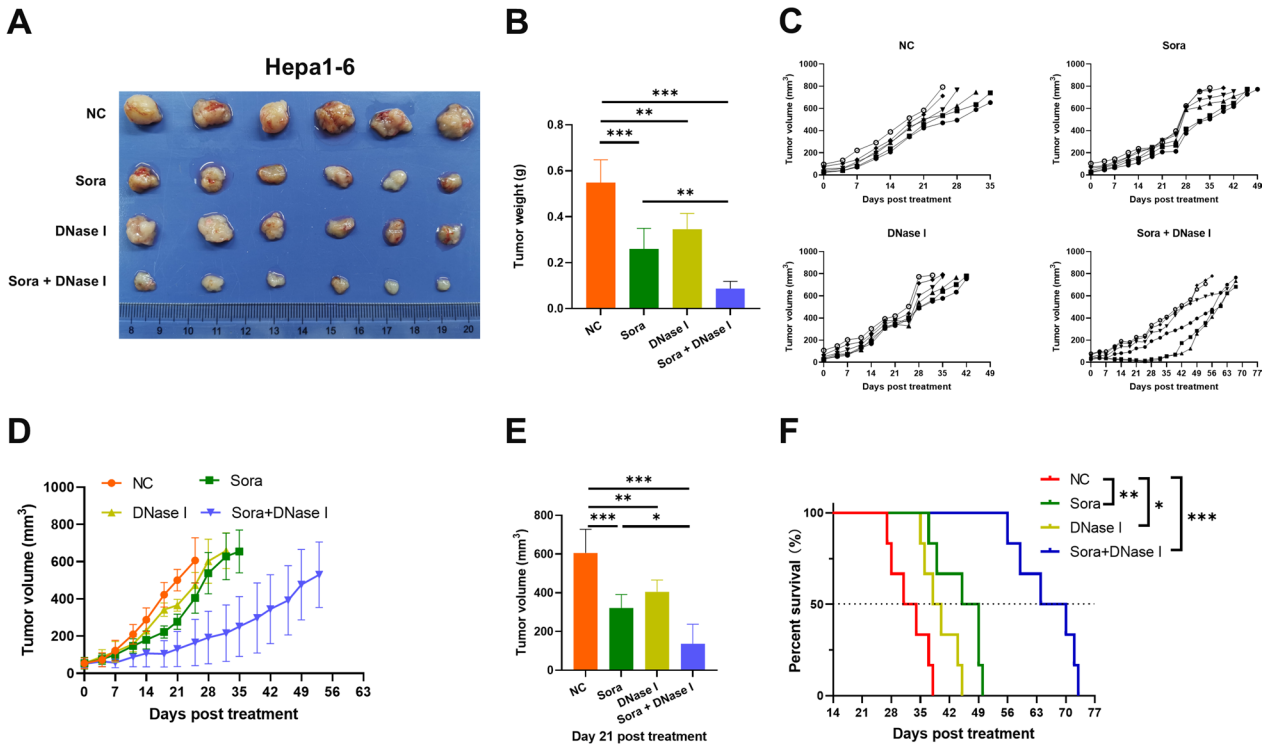


**Fig. 2** The role of METs in sorafenib resistance in HCC. **A** Tumor photos and **B** tumor weight in Hepa1-6 model of HCC. NC: negative control with saline treatment. Sora: treatment with sorafenib. DNase I: treatment with DNase I. Sora + DNase I: treatment with sorafenib and DNase I. **C** Individual and **D** grouped tumor growth curve in Hepa1-6 model of HCC. **E** Tumor volume in Hepa1-6 model of HCC on day 25 after the first subcutaneous injection. **F** Survival of Hepa1-6 model of HCC. n = 6 **B**–**F**. Statistical significance was calculated by one-way analysis of variance (ANOVA), followed by Tukey's multiple comparisons test **B** and **E**, and Log-rank (Mantel-Cox) test. Data represent the mean ± standard deviation (SD) of ≥ three independent experiments. *, $p < 0.05$; **, $p < 0.01$; ***, $p < 0.001$

combination therapy brought a 78% reduction (Fig. 2E). Consistently, the combination therapy surpassed single treatment in offering survival benefits in the mice (Fig. 2F). These results suggested the essential role of METs in mediating sorafenib resistance in HCC.

### Sorafenib induced MET formation via promoting IL4 expression in HCC cells

Based on the above-mentioned findings, the mechanism underlying MET formation following sorafenib therapy was investigated. Given that CM from sorafenib-treated HCC cells could trigger MET formation, we speculated that the sorafenib promoted HCC cells to secret specific METs-induced molecules. Therefore, we screened the mRNA expression levels of macrophage activation-associated cytokines in sorafenib-treated Hep3B cells to find potential contributing components. The qPCR screening results showed the mRNA expression level of IL4, the M2 macrophage polarization cytokine [44], was markedly increased by sorafenib in Hep3B cells (Fig. 3A). The ELISA results showed that sorafenib dramatically elevated IL4 concentration in Hep1-6 and Hep3B culture media as early as 12 h after sorafenib treatment (Fig. 3B), further supporting a promoted IL4 secretion of HCC cells after sorafenib treatment. At this point, sorafenib-induced cell death was unobservable (Fig. S2A-B).

We then asked whether HCC cell-derived IL4 mediates sorafenib-induced MET formation. We found that IL-4 could directly induce MET formation by M2-mBMDM and M2-THP-1 (Fig. 3C). The results from in vitro MET formation experiments further showed that inhibiting IL4 (IL4-IN) by neutralizing antibodies abolished the MET formation caused by the CM of either Hep3B or Hepa1-6 cells treated with sorafenib (Fig. 3D). These in vitro results encouraged us to further investigate the potential implication of IL4 in METs-mediated sorafenib resistance in HCC in vivo. The Hepa1-6 tumor-bearing mice received the administration of IgG1 isotype (NC), sorafenib and IgG1 isotype (Sora), IL4 neutralizing antibody (IL4-IN), or sorafenib and IL4 neutralizing antibody (Sora + IL4-IN). The results showed that the combination of sorafenib and IL4-IN led to a significant decrease in tumor weight compared to sorafenib or IL4-IN alone (Fig. 3E, F). We monitored tumor volumes in a parallel

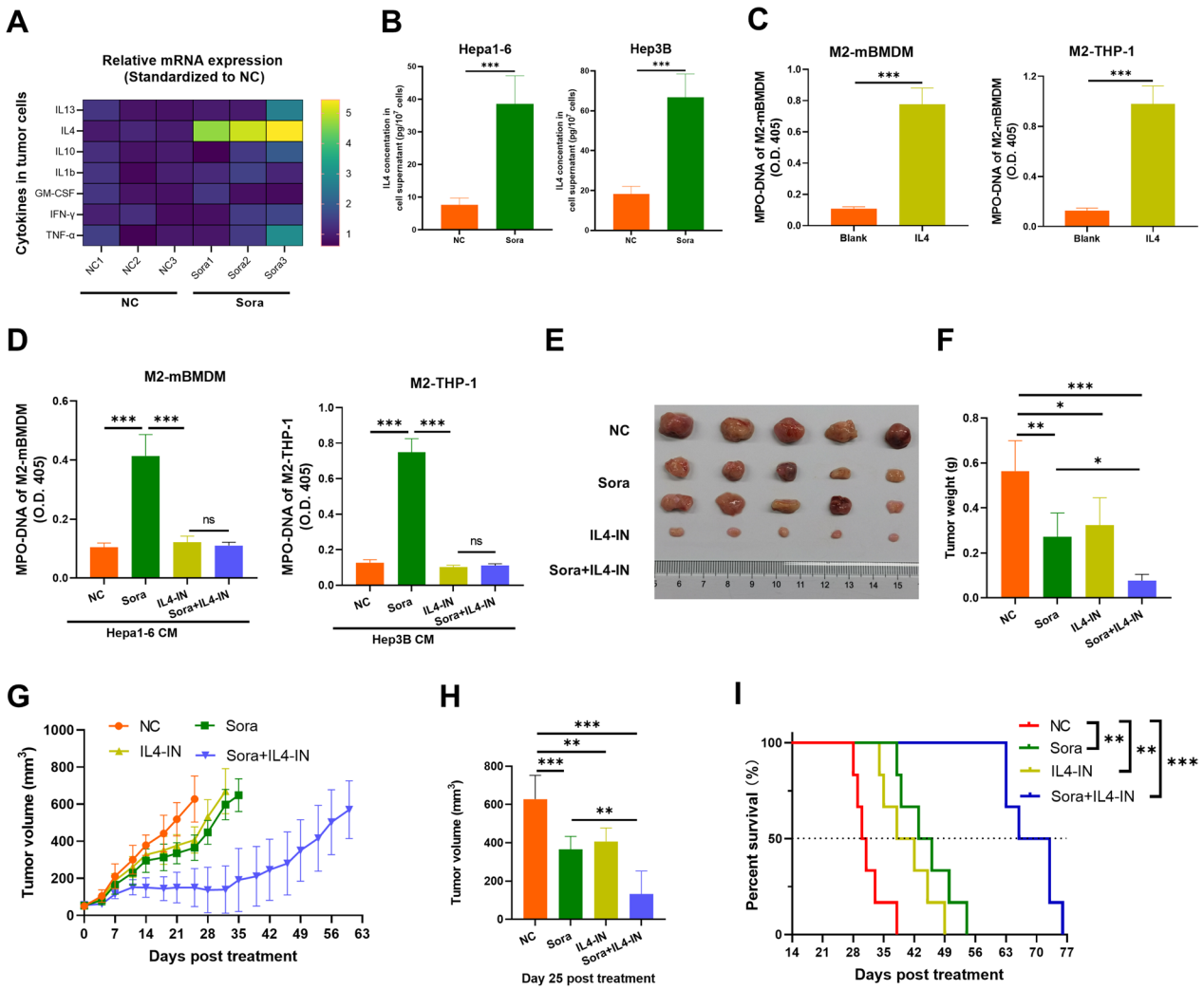


**Fig. 3** The impact of sorafenib on IL4 secretion by HCC cells, and subsequent METs-mediated drug resistance. **A** The mRNA expression levels of macrophage activation associated cytokines in Hep3B cells after sorafenib treatment. n = 3. **B** ELISA detection of IL4 concentration in Hep1-6 and Hep3B culture media. NC: negative control. Sora: Hep1-6 and Hep3B cells were incubated with sorafenib. ELISA detection of the MPO-DNA concentration in the supernatant of M2-mBMDM and M2-THP-1 cells that were treated with **C** IL4 or **D** HCC cell media. n = 6 B–D. Blank: No treatment. NC: received treatment with IgG1 isotype and the media of Hepa1-6 or Hep3B. Sora: received treatment with IgG1 isotype and the media of Hepa1-6 or Hep3B treated by sorafenib. IL4-IN: received treatment with IL4 inhibitor (IL4-IN, neutralizing antibody) and the media of Hepa1-6 or Hep3B. Sora + IL4-IN: received treatment with IL4-IN and the media of Hepa1-6 or Hep3B treated by sorafenib. **E** Tumor photos and **F** tumor weight in Hepa1-6 model of HCC. n = 5. **G** Grouped tumor growth curve in Hepa1-6 model of HCC. **H** Tumor volume in Hepa1-6 model of HCC on day 25 after the first injection. n = 6. I Survival of Hepa1-6 model of HCC. n = 6. NC: negative control, treatment with IgG1 isotype. Sora: treatment with sorafenib and IgG1 isotype. IL4-IN: IL4 inhibition with neutralizing antibody. Sora + IL4-IN: treatment with sorafenib and IL4 neutralizing antibody. Statistical significance was calculated by two-tailed student's t-test **B**, **C**, one-way analysis of variance (ANOVA) followed by Tukey's multiple comparisons test **D**, **F** and **H**, and Log-rank (Mantel-Cox) test **I**. Data represent the mean ± standard deviation (SD) of ≥ three independent experiments. *, $p < 0.05$; **, $p < 0.01$; ***, $p < 0.001$

experiment and observed similar results (Fig. 3G, H). Moreover, 3/6 of the mice showed tumor regression in response to the combination therapy of sorafenib and IL4-IN (Fig. S3A-D). Meanwhile, no tumor regression was observed in the single treatment group. Additionally, IL4-IN significantly prolonged the survival time of sorafenib-treated mice (Fig. 3I). These results hint the potential of IL4 inhibition in enhancing sorafenib response in treating HCC.

**Sorafenib triggered IL4 secretion by HCC cells via ARHGDIG**

To identify the potential molecular link between sorafenib treatment and IL4 expression in HCC cells, we analyzed the mRNA expression of genes co-expressed with IL4,

which were identified in HCC tissues based on TCGA database by GEPIA 2.0 [45] (Table S1), in sorafenib-treated Hep3B cells. Top 10 co-expressed genes, whose mRNA and amino acid sequences are verified in the NCBI Gene, were analyzed and ARHGDIG was found to be markedly upregulated in response to sorafenib treatment in HCC cell Hep3B (Fig. 4A). Mechanically, the qPCR and Western Blot assay showed that ARHGDIG-knockdown ($ARHGDIG^{knock}$) could decrease the mRNA and protein expressions of IL4, and sorafenib couldn't further increase expressions of IL4 while ARHGDIG was knocked in HCC cells (Fig. 4B, C). Western Blot assay also confirmed that sorafenib could significantly increase the protein expressions of ARHGDIG. To verify whether ARHGDIG is involved in the increase of IL4 expression induced by sorafenib, we treated the parental or ARHGDIG-knockdown ($ARHGDIG^{knock}$) Hep1-6 and Hep3B cells with sorafenib and then detected the secretion of IL4. The results from ELISA demonstrated that sorafenib could increase IL4 secretion by Hep1-6 and Hep3B cells. In contrast, the effect of sorafenib on IL4 was abolished in ARHGDIG-knockdown cells (Fig. 4D). Subsequently, we further investigate the impact of ARHGDIG on the sorafenib-induced METs. As shown, the CM from ARHGDIG-knockdown HCC cells was less potent in inducing MET formation, and ARHGDIG knockdown almost completely inhibited the enhanced MET formation caused by the CM from sorafenib-treated HCC cells as determined by detecting the MPO-DNA and elastase release by macrophages (Fig. 4E, F ), as well as SYTOX Green intensity in macrophages (Fig. 4G). These data suggest that ARHGDIG-dependent IL4 expression in tumor cells in response to sorafenib is important upstream event in sorafenib-induced MET in HCC.

#### IL4-inudced PADI4 expression in macrophage was essential for sorafenib-induced METs

We further investigated the macrophage-related mechanism of MET formation induced by the CM from sorafenib-treated HCC cells. It was reported that peptidyl arginine deiminase 2 (PADI2) and PADI4 are essential in MET formation [46–48]. Therefore, we incubated M2-mBMDM with media from Sora-treated Hepa1-6 and detected the protein expression levels of PADI4 and PADI4 in M2-mBMDM. The results showed that the protein expression level of PADI4 rather than PADI2 was markedly increased by the CM of sorafenib-treated HCC cells (Fig. 5A). We further showed that the CM from sorafenib-treated Hepa1-6 or Hep3B (Sora group) increased the mRNA expression of PADI4 in both M2-mBMDM and M2-THP-1 (Fig. 5B). As expected, treatment with IL4 neutralization antibodies resulted in a substantially lower level of PADI4 in macrophages incubated with HCC cells' CM (Fig. 5C). Meanwhile, the CM from sorafenib-treated HCC cells failed to elevate PADI4 expression after inhibition of IL4 (Fig. 5C), suggesting HCC cell-derived IL4 accounts for the increased PADI4 expression after sorafenib treatment.

We then investigated the role of PADI4 in MET formation induced by sorafenib-treated HCC cells. The results from our in vitro MET formation assay showed that PADI4 inhibitor GSK484 significantly decreased the extracellular levels of MPO-DNA and elastase in macrophage cultures after incubation with the CM from sorafenib-treated HCC cells as IL4 neutralizing antibody did (Fig. 5D, E). METs were also detected by measuring the fluorescence of the cell-impermeable DNA dye SYTOX Green. The results showed that the PADI4 inhibition and IL4 neutralization restored the fluorescence of SYTOX Green in M2-mBMDM and M2-THP-1 increased by the CM of sorafenib-treated HCC cells (Fig. 5E, F). Furthermore, there is no significant difference of MPO-DNA concentration, intensity of SYTOX Green Fluorescence and elastase concentration between Sora + IL4-IN and Sora + PADI4-IN groups, indicating the essential role of PADI4 in IL4-induced MET formation.

Given the involvement of PADI4 in sorafenib-induced MET formation, we extended our investigation into the role of PADI4 in sorafenib resistance. In the Hepa1-6 HCC tumor model, we observed that PADI4-IN significantly improved sorafenib efficiency (Fig. 5H). On day 25 after the first injection, the combination therapy exhibited a significant reduction in tumor volume compared to single sorafenib therapy (Fig. 5I and S4A–D). Additionally, PADI4 inhibition by GSK484 significantly enhanced the beneficial effect of sorafenib on survival improvement in HCC tumor-bearing mice (Fig. 5J).

#### IL4-induced METs suppressed sorafenib-induced ferroptosis of HCC cells

To explore the mechanism of METs-mediated sorafenib resistance, we investigated the effect of sorafenib-induced METs on the biological behavior of HCC cancer cells. We incubated M2-mBMDM or M2-THP-1 with the media of HCC cells (NC), the media of HCC cells treated with sorafenib (Sora), the media of HCC cells treated with sorafenib and IL4 neutralizing antibody (Sora + IL4-IN), or the media of HCC cells treated with sorafenib and PADI4 inhibitor GSK484 (Sora + PADI4-IN), and then cocultured BMDM with Hep1-6 or Hep3B cells. We then detected some biologically behavioral indicators of tumor cells. We used CCK-8 to detect the viability of cancer cells and conducted the transwell migration assay to detect the migration and ability of cancer cells. The results showed that Sora group-treated macrophages

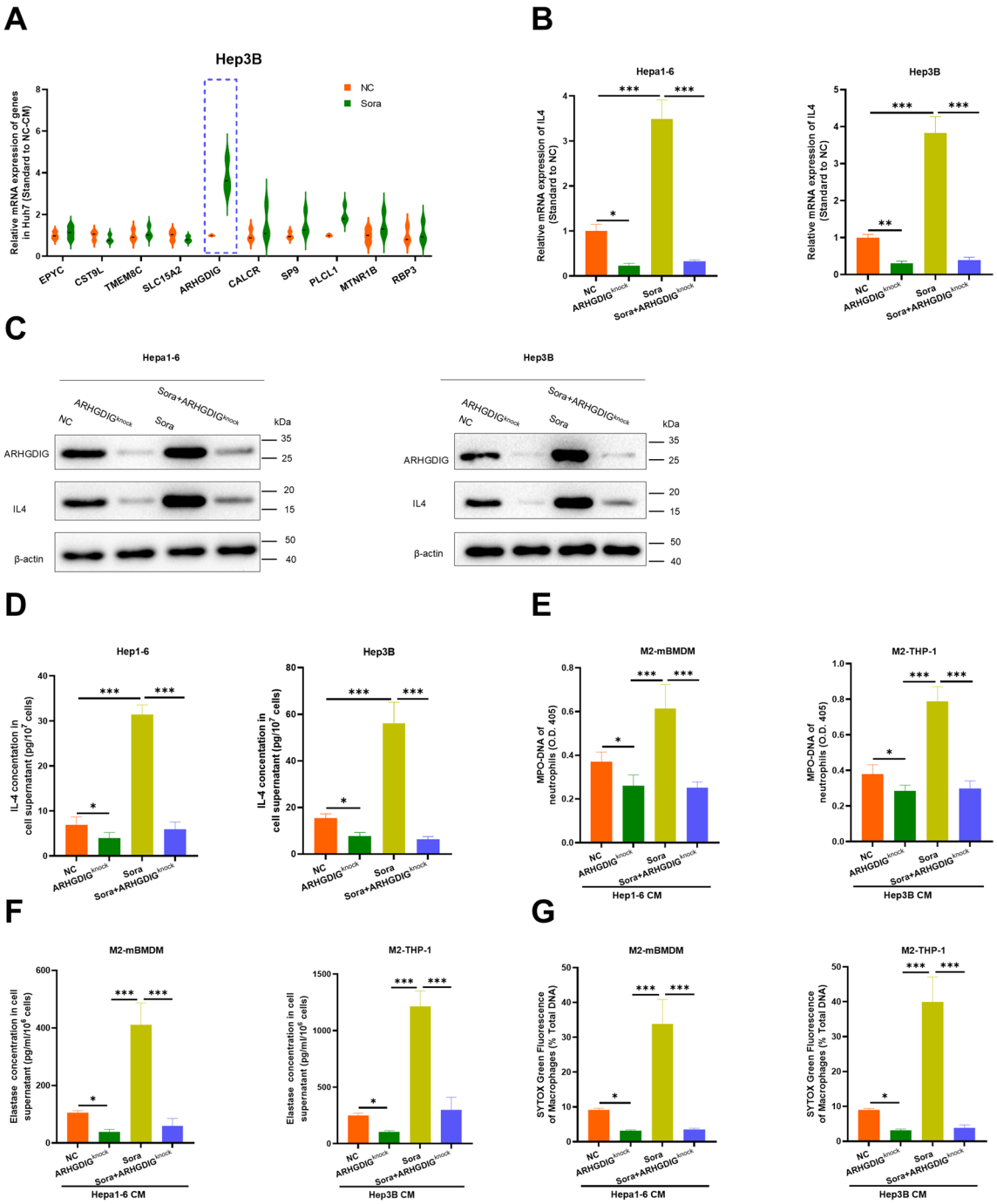


**Fig. 4** ARHGDIG-mediated IL4 release by HCC cells mediated MET formation and drug resistance. **A** The mRNA expression of candidate genes in Hep3B cells. NC: Hep3B cells received no treatment. Sora: Hep3B cells received treatment with sorafenib. n = 3. **B** The mRNA expression of IL4 in Hepa1-6 and Hep3B cells. n = 3. **C** The Western Blot assay of protein expressions of ARHGDIG and IL4 in Hep3B and Hepa1-6 cells. NC: no treatment. ARHGDIG$^{knock}$: ARHGDIG knockdown in cells. Sora: treatment with sorafenib. Sora + ARHGDIG$^{knock}$: ARHGDIG knocking cells received treatment with sorafenib. **D** ELISA detection of the IL4 concentration in the supernatant of Hepa1-6 and Hep3B cells. ELISA detection of the **E** MPO-DNA and **F** elastase concentration in the supernatant of M2-mBMDM and M2-THP-1 cells that were treated with media of HCC cell Hepa1-6 or Hep3B. **G** The intensity of SYTOX Green fluorescence in M2-mBMDM and M2-THP-1 cells that were treated with media of HCC cell Hepa1-6 or Hep3B. NC-CM: media of HCC cells. ARHGDIG$^{knock}$: media of ARHGDIG-knockdown HCC cells. Sora: media of HCC cells receiving treatment with sorafenib. Sora + ARHGDIG$^{knock}$: media of ARHGDIG-knockdown HCC cells receiving treatment with sorafenib. n = 6 (**C**–**G**). Statistical significance was calculated by one-way analysis of variance (ANOVA) followed by Tukey's multiple comparisons test (**B**, **D**–**G**). Data represent the mean ± standard deviation (SD) of ≥ three independent experiments. *, $p < 0.05$; **, $p < 0.01$; ***, $p < 0.001$

enhance cancer cells' viability (Fig. 6A) and migration ability (Fig. 6B). Macrophages treated with the media from Sora + IL4-IN and Sora + PADI4-IN groups, on the other hand, could not effectively enhance the viability and the migration ability of cancer cells.

Next, we explored the mechanism by which METs enhanced the viability and migration of HCC cells inhibited by sorafenib. The induction of tumor cell ferroptosis is believed as a main mechanism for the anti-HCC effect of sorafenib. We therefore further investigate the influence of MET on sorafenib-induced ferroptosis of HCC cells. Ferroptosis is necrotic cell death caused by iron-dependent oxidized phospholipids, leading to membrane damage and cell lysis [49], and it is particularly prevalent in HCC [50–52]. For these reasons, we further explored whether the macrophages treated with CM could influence the ferroptosis of HCC cells. Hepa1-6 cells or Hep3B cells were cocultured with M2-polarized mBMDM or THP-1-derived macrophages in the presence or absence of IL4 neutralizing antibody or DNase I in a horizontal coculture system. The cocultures of HCC cells and macrophages were treated with IL4 to induce METs and then with sorafenib to induce ferroptosis, which was determined by analyzing the intercellular levels of $Fe^{2+}$ and lipid ROS in HCC cells. The results showed that macrophages treated with IL4 could reduce the content of $Fe^{2+}$ and the level of lipid ROS in cancer cells treated with sorafenib. In contrast, macrophages treated with IL4 + PADI4-IN or IL4 + DNase I couldn't reduce the content of $Fe^{2+}$ and the level of lipid ROS in cancer cells (Fig. 6C, D). In the presence of the ferroptosis inhibitor DFO, sorafenib failed to induce lipid peroxidation of HCC cells (Fig. 6D). Notably, MET inhibition by PADI4 inhibitor GSK484 and DNase I could recover sorafenib-induced lipid peroxidation inhibited by IL4 (Sora + IL4)-induced METs. However, after treatment by the ferroptosis inhibitor DFO, METs inhibition by PADI4 inhibitor and DNase I couldn't present this effect. The Western Blot assay showed that macrophages treated with IL4 could increase the expression level of iron death regulatory protein GPX4 in cancer cells treated with sorafenib. In contrast, macrophages treated with IL4 + PADI4-IN and IL4 + DNase I couldn't effectively increase the protein expression of GPX4 in cancer cells (Fig. 6E). Additionally, we also explored the impact of METs on sorafenib-induced apoptosis and pyroptosis, finding that IL4-induced METs could suppress the ferroptosis of HCC cells induced by sorafenib, but PADI4 inhibition or DNase I couldn't reverse this suppression significantly (Fig. S5A). Meanwhile, IL4-induced MET failed to impact pyroptosis (Fig. S5B). The results indicated that METs could suppress the ferroptosis of HCC cells induced by sorafenib, while PADI4 inhibition or DNase I could reverse this suppression.

## Discussion

Chemoresistance restricts the sorafenib efficiency, intimately associated with a complex tumor immunological milieu in HCC. In this regard, we demonstrate that sorafenib treatment causes MET formation, which in turn enhances the drug resistance of HCC. Subsequently, we discover the underlying molecular mechanism that sorafenib increases IL4 secretion through ARHGDIG in HCC cells, which triggers MET formation via PADI4. Furthermore, METs promote the viability, migration, and ferroptosis of tumor cells. Importantly, the MET inhibition improved sorafenib efficiency significantly. Our findings point to METs' potential involvement in sorafenib resistance in HCC, which might be overcome by targeting the ARHGDIG/IL4/PADI4/METs axis.

(See figure on next page.)

**Fig. 5** PADI4 in macrophages mediated MET formation triggered by sorafenib/IL4. **A** Detection of protein expressions of molecules associated with MET formation in M2-mBMDM using Western Blot. NC-CM: media of Hepa1-6. Sora-CM: media of Hepa1-6 treated by sorafenib. **B** The mRNA expression of PADI4 in M2-mBMDM and M2-THP-1. NC: M2-mBMDM and M2-THP-1 received treatment from media of Hepa1-6 or Hep3B cells. Sora-CM: M2-mBMDM and M2-THP-1 received treatment from media of Hepa1-6 or Hep3B cells that were treated by sorafenib. n = 3. **C** The Western Blot assay of PADI4 protein expression in M2-mBMDM and M2-THP-1 cells that were treated with HCC cell media. NC-CM: media of Hepa1-6 or Hep3B. NC-CM + IL4-IN: received treatment with IL4 inhibitor (IL4-IN, neutralizing antibody) and NC-CM. Sora-CM: media of Hepa1-6 or Hep3B treated by sorafenib. Sora-CM + IL4-IN: received treatment with IL4-IN and Sora-CM. ELISA detection of the **D** MPO-DNA and **G** elastase concentration in the supernatant of M2-mBMDM and M2-THP-1 cells that were treated with media of HCC cell Hepa1-6 or Hep3B. **E** Microscopy detection of SYTOX Green fluorescence in M2-THP-1 cells that were treated with media of Hep3B cells. Scale bar: 400 μm. **F** The intensity of SYTOX Green fluorescence in M2-mBMDM and M2-THP-1 cells that were treated with media of HCC cell Hepa1-6 or Hep3B. NC: media of HCC cells. Sora: media of HCC cells receiving treatment with sorafenib. Sora + IL4-IN: received treatment with IL4-IN and media of HCC cells treated by sorafenib. Sora + PADI4-IN: received treatment with PADI4 inhibitor (PADI4-IN, GSK484) and media of HCC cells treated by sorafenib. **H** Tumor growth curve in Hepa1-6 model of HCC. **I** Tumor volume in Hepa1-6 model of HCC on day 25 after the first injection. **J** Survival of Hepa1-6 model of HCC. NC: negative control with saline treatment. Sora: treatment with sorafenib. PADI4-IN: treatment with PADI4 inhibitor GSK484. Sora + PADI4-IN: treatment with sorafenib and GSK484. n = 6 (**D**, **F**, **G**, **I** and **J**). Statistical significance was calculated by two-tailed student's t-test (**B**), one-way analysis of variance (ANOVA) followed by Tukey's multiple comparisons test (**D**, **F**, **G** and **I**), and Log-rank (Mantel-Cox) test (**J**). Data represent the mean ± standard deviation (SD) of ≥ three independent experiments. *, $p < 0.05$; **, $p < 0.01$; ***, $p < 0.001$

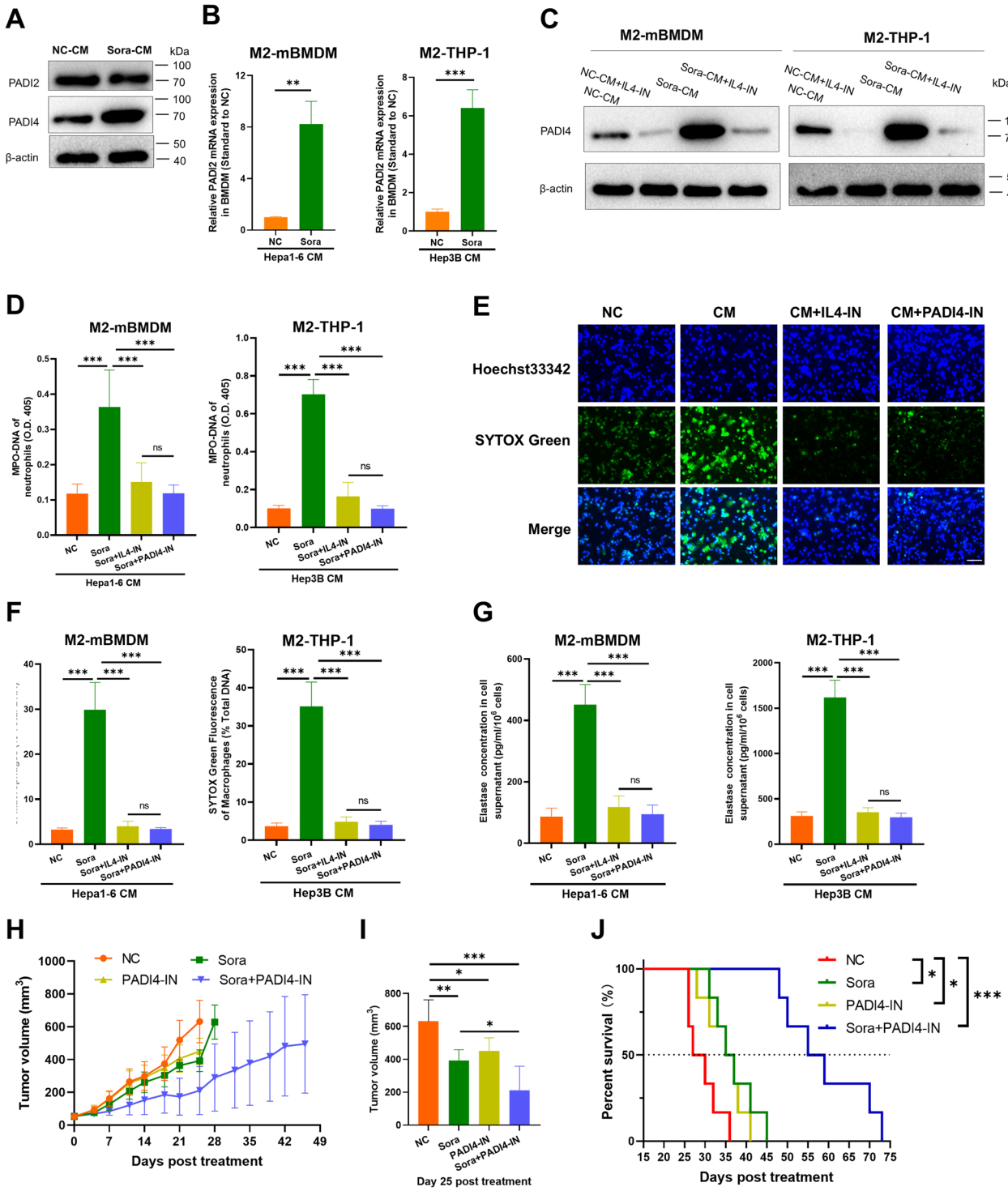


**Fig. 5** (See legend on previous page.)

We first found that sorafenib treatment could induce MET formation in the tumor microenvironment of the HCC mouse model. Firstly, we excluded the direct effect of sorafenib on MET formation through in vitro experiments. As for the indirect effect of sorafenib on MET formation, we have confirmed that sorafenib can promote MET formation through HCC cells. Of course, this does not exclude other possible pathways that are

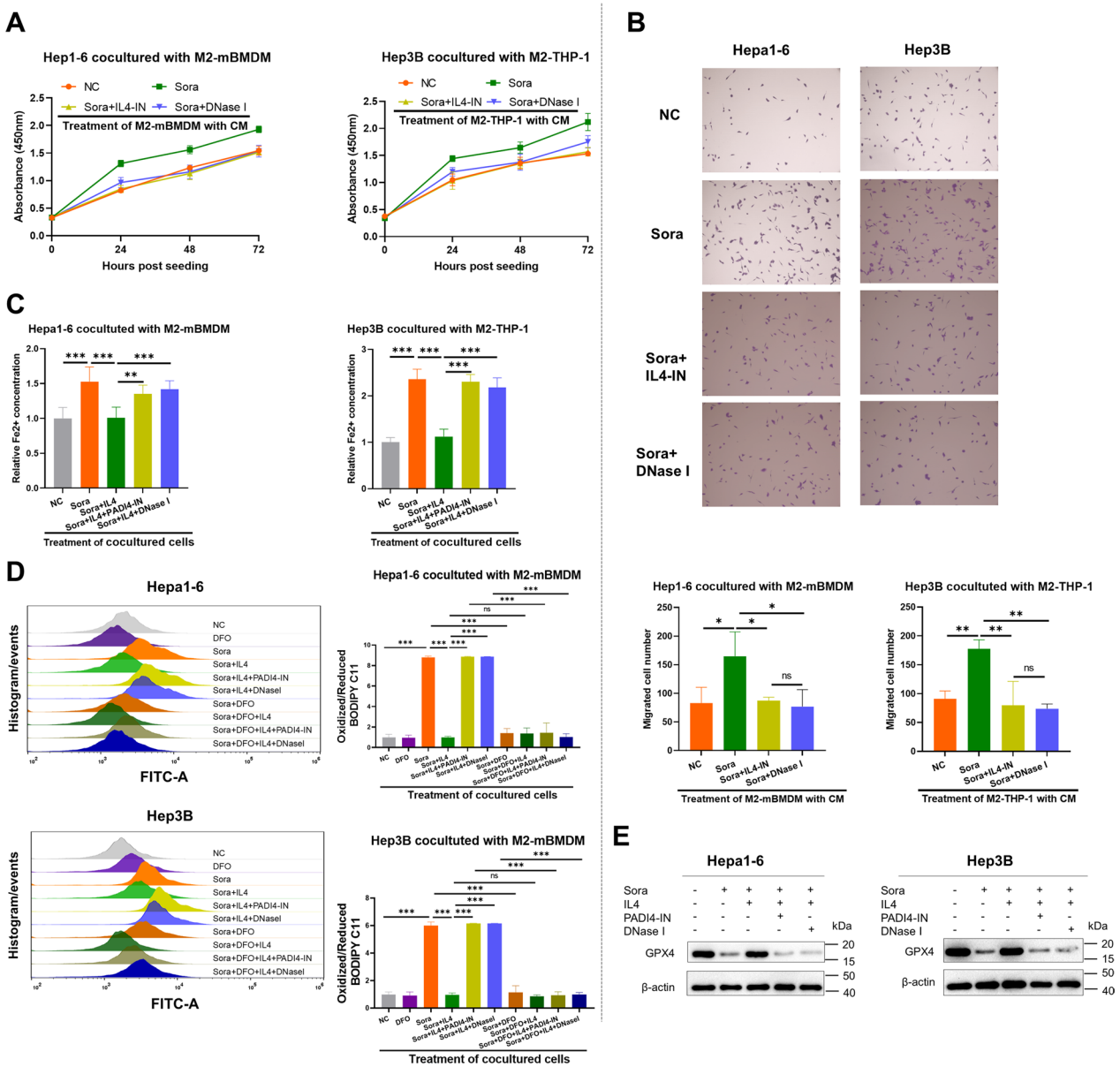


**Fig. 6** Sorafenib/IL4-induced METs enhanced ferroptosis resistance of HCC cells. **A** CCK-8 assay and **B** transwell migration assay of Hepa1-6 and Hep3B cells (100 × magnification). n = 3. **C** The content of $Fe^{2+}$ in Hepa1-6 and Hep3B cells, detected by the Iron Assay kit (Colorimetric). n = 6. **D** Detection of lipid peroxidation (lipid ROS) in Hepa1-6 and Hep3B cells with the mean fluorescence intensity (MFI) of BODIPY™ 581/591 C11 by flow cytometry. n = 3. **E** Western Blot assay of GPX4 protein expression level in Hepa1-6 and Hep3B cells. NC: HCC cells without treatment. Sora: HCC cells treated with sorafenib. DFO: HCC cells treated with deferoxamine (DFO). Sora + IL4: HCC cells were treated with sorafenib, and macrophages were treated with IL4. Sora + IL4 + PADI4-IN: HCC cells were treated with sorafenib, and macrophages were treated with IL4 and PADI4 inhibitor GSK484. Sora + IL4 + DNase I: HCC cells were treated with sorafenib, and macrophages were treated with IL4 and DNase I. Sora + DFO: HCC cells were treated with sorafenib and DFO. Sora + DFO + IL4: HCC cells were treated with sorafenib and DFO, and macrophages were treated with IL4. Sora + DFO + IL4 + PADI4-IN: HCC cells were treated with sorafenib and DFO, and macrophages were treated with IL4 and PADI4 inhibitor GSK484. Sora + DFO + IL4 + DNase I: HCC cells were treated with sorafenib and DFO, and macrophages were treated with IL4 and DNase I. Statistical significance was calculated by one-way analysis of variance (ANOVA) followed by Tukey's multiple comparisons test (B-D). Data represent the mean ± standard deviation (SD) of ≥ three independent experiments. *, $p < 0.05$; **, $p < 0.01$; ***, $p < 0.001$

involved in the impact of sorafenib on MET formation, which requires further exploration. Since neutrophils are an essential source of extracellular traps in various cancers [53–55], so we need to consider whether the elevated MPO-DNA in peripheral blood caused by sorafenib treatment derives from neutrophils. Currently, some studies have found that chemotherapy drugs can cause NET formation [56–58], and our study, for the first time, found that sorafenib could cause MET formation but has no significant effect on NET formation. In our research, sorafenib induced M2 macrophages to produce METs, but it did not show the same effect on M1 macrophages. Of course, M1 macrophages could also produce extracellular traps on exposure to phorbol myristate acetate (PMA), interleukin-8 (IL-8), and tumor necrosis factor α (TNFα) [59, 60]. Therefore, both M1 and M2 macrophages can produce METs, which might depend on different stimuli.

DNase I could remove the DNA of extracellular traps and it was administrated in diverse cancer mouse models [56, 61, 62], including liver cancer [63], has been shown to inhibit disease progression and increase survival, without causing adverse events. In the Hep1-6 HCC models, DNase I improved the efficacy of sorafenib, which not only considerably limited the growth rate of tumors but also prolonged the survival of mice. The canonical role of IL4, a prototypic immunomodulatory cytokine with a multitude of activities, is to trigger the alternative activation of macrophages, resulting in the M2 polarized phenotype [44, 64]. Currently, multiple inducers of METs have been found [59, 60], and we have confirmed for the first time that IL4 is an M2 macrophage-specific inducer of METs. IL4 plays a vital role in the field of tumor treatment. Overexpression of IL4 in Hep3B cells can inhibit the efficacy of immunotherapy while blocking IL4 can enhance the effectiveness of CAR-T [65]. Of course, cancer cells are not the main source of IL4 in vivo. The main sources of IL4 are mast cells, Th2 cells, eosinophils, and basophils [66]. Moreover, we found that the expression levels of IL4 in Hep1-6 and Hep3B cells were very low, while sorafenib could induce a significant increase in IL4 levels in cancer cells. In our study, sorafenib increased IL4 production by increasing the expression level of ARHGDIG in HCC cells. After knocking ARHGDIG, sorafenib failed to trigger IL4-induced MET formation by HCC cells. ARHGDIG belongs to Rho GDP dissociation inhibitors (RhoGDIs) family. RhoGDIs regulate GDP/GTP exchange through binding to the majority of Rho GTPases in the cytoplasm to prevent the nucleotide exchange, and thus block their activation [67]. RhoGDIs in tumor progression and metastasis remains controversial [68–70], and it was documented that the level of RhoGDI3 was identified to be similar in tumor and para-carcinoma tissues of HCC patients [71]. We first report the role of ARHGDIG in HCC cell-induced MET formation by M2 macrophages in sorafenib. Compared with the negative group, the M2 macrophages treated with the CM from sorafenib-treated HCC cells produced METs, but inhibiting PADI4 could almost block this process, indicating that PADI4 is the key molecule for the formation of METs caused by sorafenib-treated HCC cells. It was documented that both PADI2 and PADI4 are essential in MET formation [46–48]. Furthermore, in this study, we found that sorafenib/IL4 induced the MET formation by increasing the expression level of PADI4, but not by PADI2.

Sorafenib/cancer cells induced METs not only inhibit the vitality and migration ability of cancer cells but also resist ferroptosis in HCC cells, as demonstrated by detecting $Fe^{2+}$, ROS, and the ferroptosis regulatory protein GPX4. Ferroptosis is a type of controlled cell death caused by lipid peroxidation, which results in the rupture of the cell membrane, and it is particularly prevalent in HCC [50–52]. The impact of sorafenib on the ferroptosis of HCC cells is controversial. A study discovered that sorafenib could activate the NFE2L2 pathway that inhibits ferroptosis, and NRF2 inhibition increased the anticancer activity of sorafenib in HCC cells [72]. However, in another document sorafenib could induce ferroptosis in HCC cells [73]. Also, one research report states that sorafenib fails to trigger ferroptosis across various cancer cell lines, including hepatoma cells Hep3B [74]. Our research explains that sorafenib could not directly affect ferroptosis in HCC cells but still could inhibit ferroptosis in HCC cells through indirect pathways such as inducing the formation of METs. Therefore, promoting ferroptosis in HCC cells can also enhance the therapeutic effect of sorafenib. Of course, whether sorafenib has other pathways that affect ferroptosis in HCC cells remains to be explored.

In conclusion, our research uncovers a significant aspect of sorafenib therapy, revealing that it increases ARHGDIG expression, which in turn stimulates HCC cells to release IL4. This cascade of events, by elevating the amount of PADI4, leads to MET formation. These METs, in turn, confer sorafenib resistance by enhancing proliferation and migration and resisting ferroptosis of HCC cells. The combination therapy of sorafenib and MET depletion proves significantly more effective than a single treatment (Fig. 7). These findings hold immense potential in guiding the development of novel therapeutic approaches that target the IL4/ PADI4 /METs axis in macrophages, thereby overcoming sorafenib

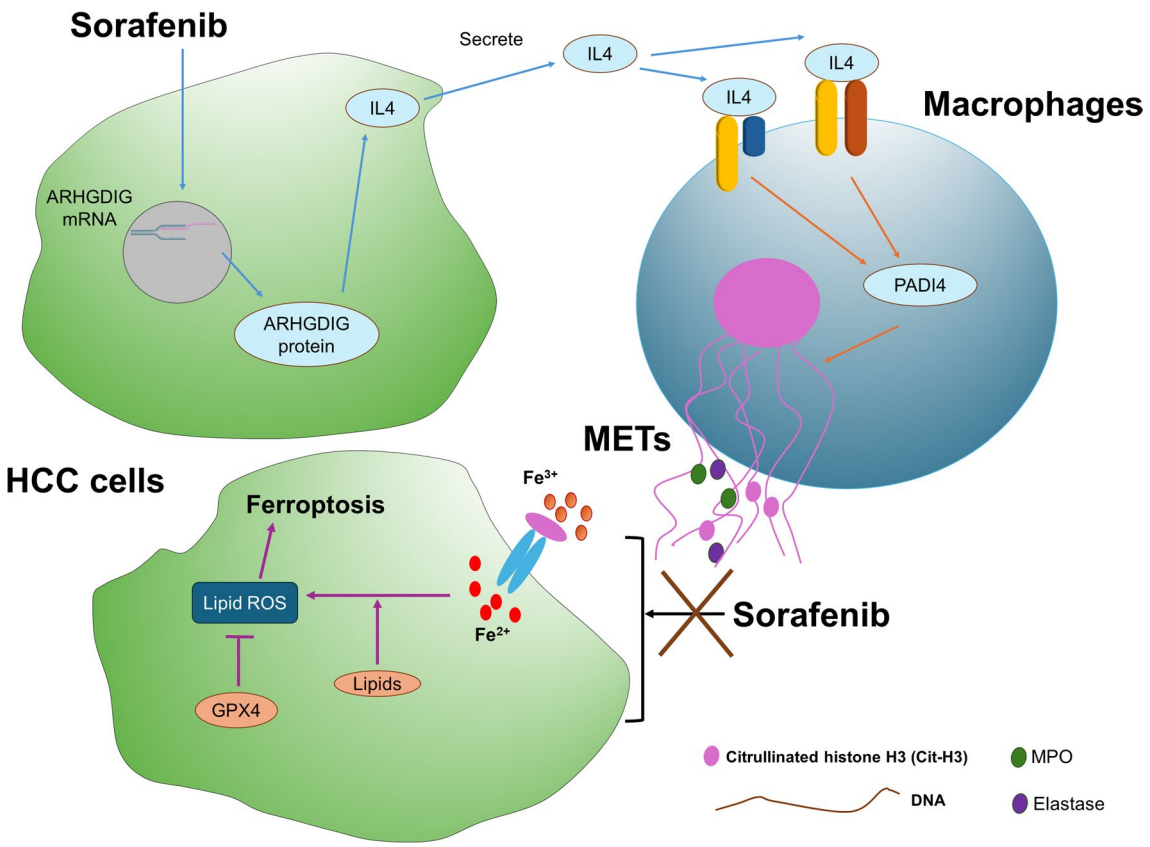


**Fig. 7** A comprehensive schematic illustrating the mechanisms by which METs contribute to sorafenib resistance in HCC. ARHGDIG expression is downregulated in HCC cells treated with sorafenib. Sorafenib increases ARHGDIG -dependent expression and secretion of IL4, which promotes MET formation via PADI4. IL4-triggered METs potently inhibited the sorafenib-induced ferroptosis of HCC cells

resistance and improving prognosis for HCC patients during treatment.

## Supplementary Information

The online version contains supplementary material available at https://doi.org/10.1186/s13062-024-00560-4.

Additional file1.

### Author contributions

X.H. designed and performed experiments, analyzed data, and wrote the original draft. J.G., N.Y. and P.Z. performed experiments and analyzed data. J.L. and J.G. supervised the project and revised the manuscript.

### Funding

This work was supported by the Henan Province Medical Science and Technology Research Program Joint Construction Project (XH, No. LHGJ20190221), Henan Province Youth Health and Health Technology Innovation Talent Training Project (JL, No. JQRC2023015), and Shanghai Sailing Program of the Science and Technology Commission of Shanghai Municipality (JG, 21YF1445300).

### Availability of data and materials

We confirm we understand the terms of the share upon reasonable request data policy, and wewill make the data freely available upon request.

## Declarations

### Ethics approval and consent to participate

The animal experiment in this study was approved by the Animal Care and Use Committee of the First Affiliated Hospital of Zhengzhou University.

### Competing interests

The authors declare no competing interests.

### Author details

[1]Department of Clinical Laboratory, The First Affiliated Hospital of Zhengzhou University, Zhengzhou 450052, People's Republic of China. [2]Key Clinical Laboratory of Henan Province, Zhengzhou 450052, People's Republic of China. [3]State Key Laboratory of Systems Medicine for Cancer, Shanghai Cancer Institute, Renji Hospital, Shanghai Jiao Tong University School of Medicine, Shanghai 200032, People's Republic of China. [4]Department of Infectious Diseases, The First Affiliated Hospital of Zhengzhou University, Zhengzhou 450052, People's Republic of China.

Received: 27 June 2024 Accepted: 4 November 2024
Published online: 11 November 2024

## References


1. Sung H, Ferlay J, Siegel RL, Laversanne M, Soerjomataram I, Jemal A, Bray F. Global cancer statistics 2020: GLOBOCAN estimates of incidence and mortality worldwide for 36 cancers in 185 countries. CA Cancer J Clin. 2021;71:209–49. https://doi.org/10.3322/caac.21660.
2. Siegel RL, Miller KD, Jemal A. Cancer statistics, 2020. CA Cancer J Clin. 2020;70:7–30. https://doi.org/10.3322/caac.21590.
3. Tang W, Chen Z, Zhang W, Cheng Y, Zhang B, Wu F, Wang Q, Wang S, Rong D, Reiter FP, et al. The mechanisms of sorafenib resistance in hepatocellular carcinoma: theoretical basis and therapeutic aspects. Signal Transduct Target Ther. 2020;5:87. https://doi.org/10.1038/s41392-020-0187-x.
4. Li Q, Chen K, Zhang T, Jiang D, Chen L, Jiang J, Zhang C, Li S. Understanding sorafenib-induced ferroptosis and resistance mechanisms: Implications for cancer therapy. Eur J Pharmacol. 2023;955: 175913. https://doi.org/10.1016/j.ejphar.2023.175913.
5. Tang D, Kroemer G, Kang R. Ferroptosis in hepatocellular carcinoma: from bench to bedside. Hepatology. 2023. https://doi.org/10.1097/HEP.0000000000000390.
6. Yau T, Kaseb A, Cheng AL, Qin S, Zhu AX, Chan SL, Melkadze T, Sukeepaisarnjaroen W, Breder V, Verset G, et al. Cabozantinib plus atezolizumab versus sorafenib for advanced hepatocellular carcinoma (COSMIC-312): final results of a randomised phase 3 study. Lancet Gastroenterol Hepatol. 2024;9:310–22. https://doi.org/10.1016/S2468-1253(23)00454-5.
7. El-Khoueiry AB, Trojan J, Meyer T, Yau T, Melero I, Kudo M, Hsu C, Kim TY, Choo SP, Kang YK, et al. Nivolumab in sorafenib-naive and sorafenib-experienced patients with advanced hepatocellular carcinoma: 5-year follow-up from CheckMate 040. Ann Oncol. 2023. https://doi.org/10.1016/j.annonc.2023.12.008.
8. Cheng K, Cai N, Zhu J, Yang X, Liang H, Zhang W. Tumor-associated macrophages in liver cancer: from mechanisms to therapy. Cancer Commun (Lond). 2022;42:1112–40. https://doi.org/10.1002/cac2.12345.
9. Zhang Q, He Y, Luo N, Patel SJ, Han Y, Gao R, Modak M, Carotta S, Haslinger C, Kind D, et al. Landscape and dynamics of single immune cells in hepatocellular carcinoma. Cell. 2019;179(829–845): e820. https://doi.org/10.1016/j.cell.2019.10.003.
10. Zheng H, Peng X, Yang S, Li X, Huang M, Wei S, Zhang S, He G, Liu J, Fan Q, et al. Targeting tumor-associated macrophages in hepatocellular carcinoma: biology, strategy, and immunotherapy. Cell Death Discov. 2023;9:65. https://doi.org/10.1038/s41420-023-01356-7.
11. Casari M, Siegl D, Deppermann C, Schuppan D. Macrophages and platelets in liver fibrosis and hepatocellular carcinoma. Front Immunol. 2023;14:1277808. https://doi.org/10.3389/fimmu.2023.1277808.
12. Dong N, Shi X, Wang S, Gao Y, Kuang Z, Xie Q, Li Y, Deng H, Wu Y, Li M, Li JL. M2 macrophages mediate sorafenib resistance by secreting HGF in a feed-forward manner in hepatocellular carcinoma. Br J Cancer. 2019;121:22–33. https://doi.org/10.1038/s41416-019-0482-x.
13. Chen Y, Ramjiawan RR, Reiberger T, Ng MR, Hato T, Huang Y, Ochiai H, Kitahara S, Unan EC, Reddy TP, et al. CXCR4 inhibition in tumor microenvironment facilitates anti-programmed death receptor-1 immunotherapy in sorafenib-treated hepatocellular carcinoma in mice. Hepatology. 2015;61:1591–602. https://doi.org/10.1002/hep.27665.
14. Huang L, Xu R, Li W, Lv L, Lin C, Yang X, Yao Y, Saw PE, Xu X. Repolarization of macrophages to improve sorafenib sensitivity for combination cancer therapy. Acta Biomater. 2023;162:98–109. https://doi.org/10.1016/j.actbio.2023.03.014.
15. Sprinzl MF, Puschnik A, Schlitter AM, Schad A, Ackermann K, Esposito I, Lang H, Galle PR, Weinmann A, Heikenwalder M, Protzer U. Sorafenib inhibits macrophage-induced growth of hepatoma cells by interference with insulin-like growth factor-1 secretion. J Hepatol. 2015;62:863–70. https://doi.org/10.1016/j.jhep.2014.11.011.
16. Wang HC, Haung LY, Wang CJ, Chao YJ, Hou YC, Yen CJ, Shan YS. Tumor-associated macrophages promote resistance of hepatocellular carcinoma cells against sorafenib by activating CXCR2 signaling. J Biomed Sci. 2022;29:99. https://doi.org/10.1186/s12929-022-00881-4.
17. Zhang W, Zhu XD, Sun HC, Xiong YQ, Zhuang PY, Xu HX, Kong LQ, Wang L, Wu WZ, Tang ZY. Depletion of tumor-associated macrophages enhances the effect of sorafenib in metastatic liver cancer models by antimetastatic and antiangiogenic effects. Clin Cancer Res. 2010;16:3420–30. https://doi.org/10.1158/1078-0432.CCR-09-2904.
18. Xu SS, Li H, Li TJ, Li S, Xia HY, Long J, Wu CT, Wang WQ, Zhang WH, Gao HL, et al. Neutrophil extracellular traps and macrophage extracellular traps predict postoperative recurrence in resectable nonfunctional pancreatic neuroendocrine tumors. Front Immunol. 2021;12: 577517. https://doi.org/10.3389/fimmu.2021.577517.
19. Chen T, Wang Y, Nan Z, Wu J, Li A, Zhang T, Qu X, Li C. Interaction between macrophage extracellular traps and colon cancer cells promotes colon cancer invasion and correlates with unfavorable prognosis. Front Immunol. 2021;12: 779325. https://doi.org/10.3389/fimmu.2021.779325.
20. Rahat MA, Galdiero MR. Editorial: extracellular traps in cancer immunity and immunotherapy. Front Immunol. 2023;14:1292819. https://doi.org/10.3389/fimmu.2023.1292819.
21. Zhu D, Lu Y, Wang Y, Wang Y. PAD4 and its inhibitors in cancer progression and prognosis. Pharmaceutics. 2022;14:2414. https://doi.org/10.3390/pharmaceutics14112414.
22. Yazdani HO, Roy E, Comerci AJ, van der Windt DJ, Zhang H, Huang H, Loughran P, Shiva S, Geller DA, Bartlett DL, et al. Neutrophil extracellular traps drive mitochondrial homeostasis in tumors to augment growth. Cancer Res. 2019;79:5626–39. https://doi.org/10.1158/0008-5472.CAN-19-0800.
23. Xia X, Zhang Z, Zhu C, Ni B, Wang S, Yang S, Yu F, Zhao E, Li Q, Zhao G. Neutrophil extracellular traps promote metastasis in gastric cancer patients with postoperative abdominal infectious complications. Nat Commun. 2022;13:1017. https://doi.org/10.1038/s41467-022-28492-5.
24. Nie M, Yang L, Bi X, Wang Y, Sun P, Yang H, Liu P, Li Z, Xia Y, Jiang W. Neutrophil extracellular traps induced by IL8 promote diffuse large B-cell lymphoma progression via the TLR9 signaling. Clin Cancer Res. 2019;25:1867–79. https://doi.org/10.1158/1078-0432.CCR-18-1226.
25. Genin M, Clement F, Fattaccioli A, Raes M, Michiels C. M1 and M2 macrophages derived from THP-1 cells differentially modulate the response of cancer cells to etoposide. BMC Cancer. 2015;15:577. https://doi.org/10.1186/s12885-015-1546-9.
26. Clever D, Roychoudhuri R, Constantinides MG, Askenase MH, Sukumar M, Klebanoff CA, Eil RL, Hickman HD, Yu Z, Pan JH, et al. Oxygen sensing by T cells establishes an immunologically tolerant metastatic niche. Cell. 2016;166(1117–1131): e1114. https://doi.org/10.1016/j.cell.2016.07.032.
27. Li L, Liu X, Sanders KL, Edwards JL, Ye J, Si F, Gao A, Huang L, Hsueh EC, Ford DA, et al. TLR8-mediated metabolic control of human treg function: a mechanistic target for cancer immunotherapy. Cell Metab. 2019;29(103–123): e105. https://doi.org/10.1016/j.cmet.2018.09.020.
28. Surolia R, Li FJ, Wang Z, Kashyap M, Srivastava RK, Traylor AM, Singh P, Dsouza KG, Kim H, Pittet JF, et al. NETosis in the pathogenesis of acute lung injury following cutaneous chemical burns. JCI Insight. 2021;6: e147564. https://doi.org/10.1172/jci.insight.147564.
29. Zhang L, Zhang K, Zhang J, Zhu J, Xi Q, Wang H, Zhang Z, Cheng Y, Yang G, Liu H, et al. Loss of fragile site-associated tumor suppressor promotes antitumor immunity via macrophage polarization. Nat Commun. 2021;12:4300. https://doi.org/10.1038/s41467-021-24610-x.
30. Shimasaki T, Yamamoto S, Omura R, Ito K, Nishide Y, Yamada H, Ohtomo K, Ishisaka T, Okano K, Ogawa T, et al. Novel platform for regulation of extracellular vesicles and metabolites secretion from cells using a multi-linkable horizontal co-culture plate. Micromach (Basel). 2021;12:1431. https://doi.org/10.3390/mi12111431.
31. Kessenbrock K, Krumbholz M, Schonermarck U, Back W, Gross WL, Werb Z, Grone HJ, Brinkmann V, Jenne DE. Netting neutrophils in autoimmune small-vessel vasculitis. Nat Med. 2009;15:623–5. https://doi.org/10.1038/nm.1959.
32. Martens CP, Van Mol P, Wauters J, Wauters E, Gangnus T, Noppen B, Callewaert H, Feyen JHM, Liesenborghs L, Heylen E, et al. Dysregulation of the kallikrein-kinin system in bronchoalveolar lavage fluid of patients with severe COVID-19. EBioMedicine. 2022;83: 104195. https://doi.org/10.1016/j.ebiom.2022.104195.
33. Donkel SJ, Wolters FJ, Ikram MA, de Maat MPM. Circulating myeloperoxidase (MPO)-DNA complexes as marker for neutrophil extracellular traps (NETs) levels and the association with cardiovascular risk factors in the general population. PLoS ONE. 2021;16: e0253698. https://doi.org/10.1371/journal.pone.0253698.

34. Vanderbeke L, Van Mol P, Van Herck Y, De Smet F, Humblet-Baron S, Martinod K, Antoranz A, Arijs I, Boeckx B, Bosisio FM, et al. Monocyte-driven atypical cytokine storm and aberrant neutrophil activation as key mediators of COVID-19 disease severity. Nat Commun. 2021;12:4117. https://doi.org/10.1038/s41467-021-24360-w.
35. Li D, Yao Y, Rao Y, Huang X, Wei L, You Z, Zheng G, Hou X, Su Y, Varghese Z, et al. Cholesterol sensor SCAP contributes to sorafenib resistance by regulating autophagy in hepatocellular carcinoma. J Exp Clin Cancer Res. 2022;41:116. https://doi.org/10.1186/s13046-022-02306-4.
36. Xu J, Ji L, Liang Y, Wan Z, Zheng W, Song X, Gorshkov K, Sun Q, Lin H, Zheng X, et al. CircRNA-SORE mediates sorafenib resistance in hepatocellular carcinoma by stabilizing YBX1. Signal Transduct Target Ther. 2020;5:298. https://doi.org/10.1038/s41392-020-00375-5.
37. Mishra PK, Patel N, Wu W, Bleich D, Gause WC. Prevention of type 1 diabetes through infection with an intestinal nematode parasite requires IL-10 in the absence of a Th2-type response. Mucosal Immunol. 2013;6:297–308. https://doi.org/10.1038/mi.2012.71.
38. Gaya M, Barral P, Burbage M, Aggarwal S, Montaner B, Warren Navia A, Aid M, Tsui C, Maldonado P, Nair U, et al. Initiation of antiviral B cell immunity relies on innate signals from spatially positioned NKT cells. Cell. 2018;172(517–533): e520. https://doi.org/10.1016/j.cell.2017.11.036.
39. Cedervall J, Dragomir A, Saupe F, Zhang Y, Arnlov J, Larsson E, Dimberg A, Larsson A, Olsson AK. Pharmacological targeting of peptidylarginine deiminase 4 prevents cancer-associated kidney injury in mice. Oncoimmunology. 2017;6: e1320009. https://doi.org/10.1080/2162402X.2017.1320009.
40. Umbricht CA, Koster U, Bernhardt P, Gracheva N, Johnston K, Schibli R, van der Meulen NP, Muller C. Alpha-PET for prostate cancer: preclinical investigation using (149)Tb-PSMA-617. Sci Rep. 2019;9:17800. https://doi.org/10.1038/s41598-019-54150-w.
41. Xiao Q, Yan L, Han J, Yang S, Tang Y, Li Q, Lao X, Chen Z, Xiao J, Zhao H, et al. Metabolism-dependent ferroptosis promotes mitochondrial dysfunction and inflammation in CD4(+) T lymphocytes in HIV-infected immune non-responders. EBioMedicine. 2022;86: 104382. https://doi.org/10.1016/j.ebiom.2022.104382.
42. Zhao Q, Chen DP, Chen HD, Wang YZ, Shi W, Lu YT, Ren YZ, Wu YK, Pang YH, Deng H, et al. NK-cell-elicited gasdermin-D-dependent hepatocyte pyroptosis induces neutrophil extracellular traps that facilitates HBV-related acute-on-chronic liver failure. Hepatology. 2024. https://doi.org/10.1097/HEP.0000000000000868.
43. Yang L, Liu Q, Zhang X, Liu X, Zhou B, Chen J, Huang D, Li J, Li H, Chen F, et al. DNA of neutrophil extracellular traps promotes cancer metastasis via CCDC25. Nature. 2020;583:133–8. https://doi.org/10.1038/s41586-020-2394-6.
44. Locati M, Curtale G, Mantovani A. Diversity, mechanisms, and significance of macrophage plasticity. Annu Rev Pathol. 2020;15:123–47. https://doi.org/10.1146/annurev-pathmechdis-012418-012718.
45. Tang Z, Kang B, Li C, Chen T, Zhang Z. GEPIA2: an enhanced web server for large-scale expression profiling and interactive analysis. Nucleic Acids Res. 2019;47:W556–60. https://doi.org/10.1093/nar/gkz430.
46. El Shikh MEM, El Sayed R, Nerviani A, Goldmann K, John CR, Hands R, Fossati-Jimack L, Lewis MJ, Pitzalis C. Extracellular traps and PAD4 released by macrophages induce citrullination and auto-antibody production in autoimmune arthritis. J Autoimmun. 2019;105: 102297. https://doi.org/10.1016/j.jaut.2019.06.008.
47. Bashar SJ, Holmes CL, Shelef MA. Macrophage extracellular traps require peptidylarginine deiminase 2 and 4 and are a source of citrullinated antigens bound by rheumatoid arthritis autoantibodies. Front Immunol. 2024;15:1167362. https://doi.org/10.3389/fimmu.2024.1167362.
48. Vossenaar ER, Radstake TR, van der Heijden A, van Mansum MA, Dieteren C, de Rooij DJ, Barrera P, Zendman AJ, van Venrooij WJ. Expression and activity of citrullinating peptidylarginine deiminase enzymes in monocytes and macrophages. Ann Rheum Dis. 2004;63:373–81. https://doi.org/10.1136/ard.2003.012211.
49. Riegman M, Sagie L, Galed C, Levin T, Steinberg N, Dixon SJ, Wiesner U, Bradbury MS, Niethammer P, Zaritsky A, Overholtzer M. Ferroptosis occurs through an osmotic mechanism and propagates independently of cell rupture. Nat Cell Biol. 2020;22:1042–8. https://doi.org/10.1038/s41556-020-0565-1.
50. Li X, Meng F, Wang H, Sun L, Chang S, Li G, Chen F. Iron accumulation and lipid peroxidation: implication of ferroptosis in hepatocellular carcinoma. Front Endocrinol (Lausanne). 2023;14:1319969. https://doi.org/10.3389/fendo.2023.1319969.
51. Wang S, Zhu L, Li T, Lin X, Zheng Y, Xu D, Guo Y, Zhang Z, Fu Y, Wang H, et al. Disruption of MerTK increases the efficacy of checkpoint inhibitor by enhancing ferroptosis and immune response in hepatocellular carcinoma. Cell Rep Med. 2024;5: 101415. https://doi.org/10.1016/j.xcrm.2024.101415.
52. Du Y, Zhou Y, Yan X, Pan F, He L, Guo Z, Hu Z. APE1 inhibition enhances ferroptotic cell death and contributes to hepatocellular carcinoma therapy. Cell Death Differ. 2024. https://doi.org/10.1038/s41418-024-01270-0.
53. Adrover JM, McDowell SAC, He XY, Quail DF, Egeblad M. NETworking with cancer: the bidirectional interplay between cancer and neutrophil extracellular traps. Cancer Cell. 2023;41:505–26. https://doi.org/10.1016/j.ccell.2023.02.001.
54. Chen Y, Hu H, Tan S, Dong Q, Fan X, Wang Y, Zhang H, He J. The role of neutrophil extracellular traps in cancer progression, metastasis and therapy. Exp Hematol Oncol. 2022;11:99. https://doi.org/10.1186/s40164-022-00345-3.
55. Song M, Zhang C, Cheng S, Ouyang D, Ping Y, Yang J, Zhang Y, Tang Y, Chen H, Wang QJ, et al. DNA of neutrophil extracellular traps binds TMCO6 to impair CD8+ T-cell immunity in hepatocellular carcinoma. Cancer Res. 2024. https://doi.org/10.1158/0008-5472.CAN-23-2986.
56. Li Y, Wu S, Zhao Y, Dinh T, Jiang D, Selfridge JE, Myers G, Wang Y, Zhao X, Tomchuck S, et al. Neutrophil extracellular traps induced by chemotherapy inhibit tumor growth in murine models of colorectal cancer. J Clin Invest. 2024;134: e175031. https://doi.org/10.1172/JCI175031.
57. Mousset A, Lecorgne E, Bourget I, Lopez P, Jenovai K, Cherfils-Vicini J, Dominici C, Rios G, Girard-Riboulleau C, Liu B, et al. Neutrophil extracellular traps formed during chemotherapy confer treatment resistance via TGF-beta activation. Cancer Cell. 2023;41(757–775): e710. https://doi.org/10.1016/j.ccell.2023.03.008.
58. Saw PE, Chen J, Song E. ChemoNETosis: a road to tumor therapeutic resistance. Cancer Cell. 2023;41:655–7. https://doi.org/10.1016/j.ccell.2023.03.011.
59. Rayner BS, Zhang Y, Brown BE, Reyes L, Cogger VC, Hawkins CL. Role of hypochlorous acid (HOCl) and other inflammatory mediators in the induction of macrophage extracellular trap formation. Free Radic Biol Med. 2018;129:25–34. https://doi.org/10.1016/j.freeradbiomed.2018.09.001.
60. Jensen M, Thorsen NW, Hallberg LAE, Hagglund P, Hawkins CL. New insight into the composition of extracellular traps released by macrophages exposed to different types of inducers. Free Radic Biol Med. 2023;202:97–109. https://doi.org/10.1016/j.freeradbiomed.2023.03.025.
61. Hawes MC, Wen F, Elquza E. Extracellular DNA: a bridge to cancer. Cancer Res. 2015;75:4260–4. https://doi.org/10.1158/0008-5472.CAN-15-1546.
62. Wang Z, Chen C, Shi C, Zhao X, Gao L, Guo F, Han M, Yang Z, Zhang J, Tang C, et al. Cell membrane derived liposomes loaded with DNase I target neutrophil extracellular traps which inhibits colorectal cancer liver metastases. J Control Release. 2023;357:620–9. https://doi.org/10.1016/j.jconrel.2023.04.013.
63. Sugihara S, Yamamoto T, Tanaka H, Kambara T, Hiraoka T, Miyauchi Y. Deoxyribonuclease treatment prevents blood-borne liver metastasis of cutaneously transplanted tumour cells in mice. Br J Cancer. 1993;67:66–70. https://doi.org/10.1038/bjc.1993.10.
64. Dang B, Gao Q, Zhang L, Zhang J, Cai H, Zhu Y, Zhong Q, Liu J, Niu Y, Mao K, et al. The glycolysis/HIF-1alpha axis defines the inflammatory role of IL-4-primed macrophages. Cell Rep. 2023;42: 112471. https://doi.org/10.1016/j.celrep.2023.112471.
65. Wang Y, Jiang H, Luo H, Sun Y, Shi B, Sun R, Li Z. An IL-4/21 inverted cytokine receptor improving CAR-T cell potency in immunosuppressive solid-tumor microenvironment. Front Immunol. 2019;10:1691. https://doi.org/10.3389/fimmu.2019.01691.
66. Allen JE. IL-4 and IL-13: regulators and effectors of wound repair. Annu Rev Immunol. 2023;41:229–54. https://doi.org/10.1146/annurev-immunol-101921-041206.
67. Akbarzadeh M, Flegel J, Patil S, Shang E, Narayan R, Buchholzer M, Kazemein Jasemi NS, Grigalunas M, Krzyzanowski A, Abegg D, et al. The pseudo-natural product Rhonin targets RHOGDI. Angew Chem Int Ed Engl. 2022;61: e202115193. https://doi.org/10.1002/anie.202115193.
68. Ding J, Huang S, Wu S, Zhao Y, Liang L, Yan M, Ge C, Yao J, Chen T, Wan D, et al. Gain of miR-151 on chromosome 8q24.3 facilitates tumour cell

migration and spreading through downregulating RhoGDIA. Nat Cell Biol. 2010;12:390–9. https://doi.org/10.1038/ncb2039.
69. Wang H, Wang B, Liao Q, An H, Li W, Jin X, Cui S, Zhao L. Overexpression of RhoGDI, a novel predictor of distant metastasis, promotes cell proliferation and migration in hepatocellular carcinoma. FEBS Lett. 2014;588:503–8. https://doi.org/10.1016/j.febslet.2013.12.016.
70. Li C, Tan YX, Zhou H, Ding SJ, Li SJ, Ma DJ, Man XB, Hong Y, Zhang L, Li L, et al. Proteomic analysis of hepatitis B virus-associated hepatocellular carcinoma: identification of potential tumor markers. Proteomics. 2005;5:1125–39. https://doi.org/10.1002/pmic.200401141.
71. Lai MC, Zhu QQ, Owusu-Ansah KG, Zhu YB, Yang Z, Xie HY, Zhou L, Wu LM, Zheng SS. Prognostic value of Rho GDP dissociation inhibitors in patients with hepatocellular carcinoma following liver transplantation. Oncol Lett. 2017;14:1395–402. https://doi.org/10.3892/ol.2017.6333.
72. Sun X, Ou Z, Chen R, Niu X, Chen D, Kang R, Tang D. Activation of the p62-Keap1-NRF2 pathway protects against ferroptosis in hepatocellular carcinoma cells. Hepatology. 2016;63:173–84. https://doi.org/10.1002/hep.28251.
73. Liu MR, Shi C, Song QY, Kang MJ, Jiang X, Liu H, Pei DS. Sorafenib induces ferroptosis by promoting TRIM54-mediated FSP1 ubiquitination and degradation in hepatocellular carcinoma. Hepatol Commun. 2023;7:e0246. https://doi.org/10.1097/HC9.0000000000000246.
74. Zheng J, Sato M, Mishima E, Sato H, Proneth B, Conrad M. Sorafenib fails to trigger ferroptosis across a wide range of cancer cell lines. Cell Death Dis. 2021;12:698. https://doi.org/10.1038/s41419-021-03998-w.

## Publisher's Note